Chin.J.Geochem.(2010)29:343–354
DOI: 10.1007/s11631-010-0466-2

Mineralogy and radioactivity of pegmatites from South Wadi Khuda area, Eastern Desert, Egypt

Mohamed F. Raslan*, Mohamed A. Ali, and Mohamed G. El-Feky
Nuclear Materials Authority, P.O. Box 530, El Maadi, Cairo, Egypt
** Corresponding author, E-mail: raslangaines@hotmail.com*

Received January 2, 2010; accepted April 1, 2010

Abstract Radioactive minerals in pegmatites associated with granitic rocks are commonly encountered in the south of the Wadi Khuda area and found as dyke-like and small bodies. They are observed within garnet-muscovite granites near the contact with older granitoids. Field surveys indicated that the studied pegmatites vary in dimensions ranging from 2 to 10 m in width and from 10 to 500 m in length. They are composed mainly of intergrowth of milky quartz, reddish-pink K-feldspar and plagioclase together with small pockets of muscovite.

Field radiometric measurements indicated that radioactivity in pegmatites is more than twice that of their enclosing country rocks. Radionuclide measurements revealed that the average contents of U and Th increase gradually from rocks of dioritic to granodioritic composition (1.5×10^{-6} U and 4.3×10^{-6} Th) and increase significantly in biotite granites (5.8×10^{-6} U and 15.2×10^{-6} Th) but drastically decrease in muscovite granites (2.2×10^{-6} U and 5.6×10^{-6} Th). The average contents of U and Th of anomalous pegmatites are 95.3×10^{-6} and 116.9×10^{-6}, respectively, indicating their uraniferous nature. In the south of the Wadi Khuda area, pegmatites are low in average Th/U (1.4) and high in average U/K (35.6), which suggests that uranium concentrating processes did not affect the pegmatites, indicating poor source-rocks.

Mineralogical investigations of the studied pegmatites revealed the presence of secondary uranium minerals (kasolite and autunite), in addition to zircon, thorite, apatite, garnet and biotite. Primary and secondary radioactive mineralizations indicated that the mineralization is not only magmatic, but also post-magmatic. Electron microprobe analyses showed distinct cryptic chemical zoning within thorite where UO_2 decreases from core to rim. This feature in thorite is sporadic, suggesting non-uniform redistributions of UO_2 within thorite during magmatic processes.

Key words radionuclide; kasolite; thorite; zircon; pegmatites; Eastern Desert; Egypt

1 Introduction

Egyptian granitic rocks of the Pan-African age account for about 40% of the exposed Precambrian of the Eastern Desert and Sinai. They are subdivided into two distinct major groups, namely the older and the younger granites. The older granites have been referred to as grey granites (Hume, 1935; El-Ramly and Akaad, 1960), and G1-granites (Hussein et al., 1982). They were emplaced around 930–850 Ma ago, and extended to 711 Ma (El-Manharawy, 1977; Dixon, 1981; Hassan and Hashad, 1990). On the other hand, the younger granites (accounting for about 30% of the area) were previously mapped as the Gattarian granites (Hume, 1935), red and pink granites (El-Ramly and Akaad, 1960), and G-II to G-III granites (Hussein et al., 1982). They were emplaced around 622–430 Ma ago (El-Manharawy, 1977; Dixon, 1981; Hassan and Hashad, 1990; Moussa et al., 2008).

The majority of radioactive occurrences in the basement rocks of Egypt are located in the younger granites and associated pegmatites. The latter have been considered as favorable uranium and thorium mineralization environments (Page, 1950). Radioactive pegmatites have been recorded in many localities in the Eastern Desert of Egypt; e.g. the pegmatitic bodies of the Gabal Ras Baroud younger granites (Sayyah et al., 1993: Raslan et al., 2010) uranium and columbite mineralization in the pegmatites related to the Gabal Abu Dob younger granites (Ibrahim et al., 1997), and radioactive pegmatites related to the Gabal El-Sibai alkali feldspar granites (Ali, 2001). Anomalous pegmatites associated with granitic rocks have also been reported in the southern part of the Eastern Desert (Ibrahim et al., 2001; Ali et al., 2005; Abdel Warith el al., 2007). The high level of radioactivity of these rocks is attributed to the presence of accessory minerals such as zircon, monazite, thorite, uran-

othorite and allanite (Shurmann, 1966). Uranium and thorium are generally enriched in the youngest, most felsic and most potassic members of comagmatic suites of igneous rocks (Rogers and Adams, 1969).

According to Cerny's (1990) pegmatite classification, the rare-earth element (REE) subclass is characterized by the niobium-yttrium-fluorine (NYF) and zirconium-niobium-fluorine (ZNF) family signatures. The NYF pegmatites are distinguished by the signature Y, Nb > Ta, HREE, U, Th, and F, whereas the ZNF pegmatites are distinguished by the signature Zr, Nb >> Ta, Y, Th, P, and F. From the viewpoint of exploration, post-orogenic, A_2-type granites are the most favorable sites for the localization of rare-metal pegmatitic mineralization of NYF affinity. These granites are characterized by mineralogical and geochemical signatures, i.e., they are transolvus, alkaline, and metaluminous to mildy peraluminous with annite-siderophyllite mica as a sole mafic mineral (Abdalla and El Afandy, 2003).

Several studies worldwide have revealed the presence of granite-pegmatite-hosted rare-metal mineralizations (Matsubara et al., 1995; Hanson et al., 1998; Erict, 2005; William et al., 2006; Pal et al., 2007).

The aim of the present study is to investigate the geology, mineralogy and radioactivity of pegmatites in the south of the Wadi Khuda area. This area is bounded by latitudes 23º36′ and 23º43′N and longitudes 35º15′ and 35º26′E. It is located about 55 km south-west of Baranis City along the Red Sea and Wadi Khuda roads (Fig. 1A). The main geological features of the area, especially their tectonic evolution, were previously studied. The Um Atali pluton is composed mainly of biotite granites with a recorded K-Ar age of (625±24 Ma) for biotite (Abdel Karim and Arva Sos., 2000).

2 Methodology

The modified geologic map (Abdel Khalek et al., 1999) in Fig. 1B was used as a base map for the whole area. More than 30 samples were collected from different rock varieties in the studied area (older granitoids, younger granite and associated pegmatites) for radiometric and petrographic invesitgations. In order to determine the petrographic characteristics of these rocks, 15 thin sections were prepared and have been firstly studied. Uranium, thorium, radium and potassium contents are determined radios metrically by using a multichanael analyzer of γ-ray detector (Gamma-Spectrometer technique). The instrument used in determination of the four radioactive elements consists of a Bicron scintillation detector NaI (Tl) 76 mm × 76 mm, hermetically sealed with the photomultiplier tube in aluminum housing. The tube is protected by a copper cylinder protection of thickness 0.6 cm against induced X ray and a chamber of lead bricks against environmental radiation.

Uranium, thorium, radium and potassium were measured by using four energy regions representing ^{234}Th, ^{212}Pb, ^{214}Pb and ^{40}K at 93 kV, 239 kV, 352 kV, and 1460 kV for uranium, thorium, radium and potassium, respectively. The measurements were carried out in sample plastic containers, cylindrical in shape, 212.6 cm^3 in volume with 9.5-cm average diameter and 3-cm height. The rock sample was crushed as fine as about 1 mm in grain size, and then the container was filled with about 300–400 gm of the crushed sample sealed well and left for at least 21 days to accumulate free radon to attain radioactive equilibrium. The relation between the percentage of ^{222}Rn accumulation and time increased till reaching the steady stage after about 38 days (Matolin, 1991). Pegmatite samples (~10 kg) were collected from the pegmatite pockets in the area representing the highest field radioactivity measurements for radiometric, petrographic and mineralogical examination, respectively. The pegmatite samples were subjected to various mineral separation steps: disintegration (crushing, grinding), desliming, and sieving, followed by heavy liquid separation using bromoform (specific gravity: 2.85). The heavy minerals were identified by X-ray diffraction (XRD) techniques and were analyzed using an Environmental Scanning Electron Microscope (ESEM) supported by energy despressive spectrometer (EDS) unit (model Philips XL 30 ESEM) at the laboratory of the Nuclear Materials Authority (NMA). The instrument enables analyses of wet, oily, dirty, nonconductive and rough samples in their natural state without modification or preparation. However, the application is limited to qualitative and semiquatntitative determinations. The analytical conditions were 25–30 kV, accelerating voltages, 1–2 micron beam diameter and 60–120 second counting time at pressures as high as 0.3–0.5 ($\times 10^5$ Pa). Minimum detectable weight concentrations of elements from 0.1 wt% to 1 wt% were obtained. Precision well below 1%, the relative accuracy of quantitative result 2%–10% for elements Z>9 (F), and 10%–20% for the light elements B, C, N, O and F.

Polished thin sections of grains separated from pegmatites were studied under reflected and transmitted light. Backscattered electron images were collected with the scanning electron microscope-energy dispersive spectrometer (BSE) (model JEOL 6400 SEM) at the Microscopy and Microanalyses Facility, University of New Brunswick (UNB), Fredericton, New Brunswick, Canada. The chemical compositions of kasolite and thorite were analyzed using the JEOL JXA-733 Superprobe, at 15 kV, with a beam current of 50 nA and peak counting time was 30 second for all

elements. Standards were: jadeite, kaersutite, quartz, and apatite (for Na, Al, Si, P, and Ca, respectively), $SrTiO_3$ (for Ti), CaF_2 (for F), Fe, Nb, Hf, Ta, Sn, Th, and U metals (for Fe, Nb, Hf, Ta, Sn, Th, and U, respectively), YAG (for Y), cubic zirconia (for Zr), Al, Si-bearing glass for Ce, Sm, Pr, Er, Gd, Eu, , Dy, and Yb, and crocoite (for Pb).

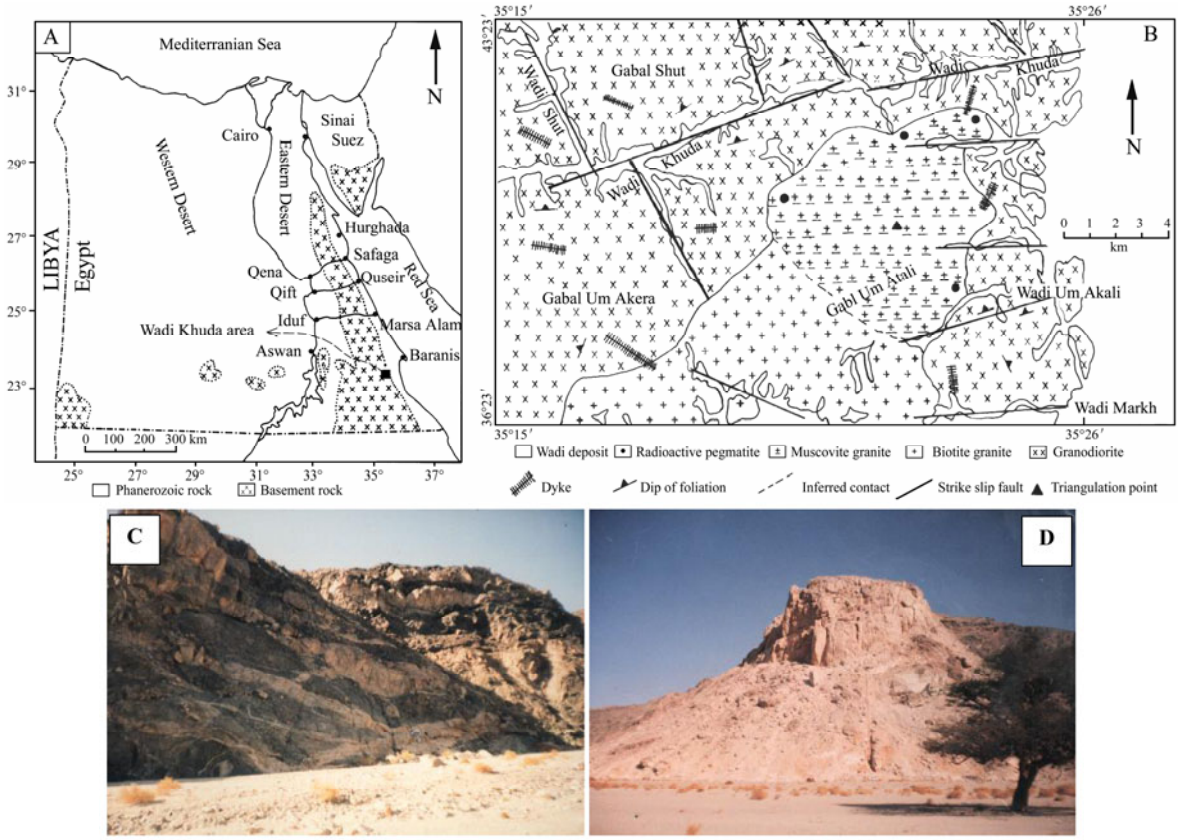

Fig. 1. A. Location map of the Wadi Khuda area; B. geological map of the Wadi Khuda area, South Eastern Desert (modified from Abdel Khalek et al., 1999); C. apophesess of muscovite granite within the older granitoids, Wadi Khuda; D. pegmatite dyke of quartz and feldspars within garnet-muscovite granites, Wadi Khuda.

3 Field geology and petrography

3.1 Diorite to granodiorite rocks

Diorite and granodiorite rocks represent the oldest lithologic unit exposed in the studied area. They crop out in a large elongated belt that tends to follow the NE-SW direction along the northern, western and eastern borders of the mapped area. They are generally characterized as being relatively low and moderate in relief, strongly jointed and dark-grey to white-grey in color. They were intruded by the biotite and muscovite granites with sharp contacts between them. The diorite to granodiorite rocks were intruded from the south and east by the muscovite granite that possesses apophysess that project into the surrounding rocks (Fig. 1C).

3.1.1 Diorite

This rock is composed of hornblende, plagioclase, biotite, apatite, titanite and opaques. In a thin-section hornblende forms large subhedral crystals of olive green color and moderate pleochroism from olive green to brownish-green. It exhibits simple twinning and two sets of cleavages. Some hornblende crystals are chloritized. Plagioclase occurs as subhedral prismatic crystals of andesine to labradorite in composition. They are characterized by albite-carlsbad twinning and show moderate alteration, especially in the core. Biotite occurs as yellowish-brown to dark brown flakes. Sometimes, they are altered to chlorite and iron oxides.

3.1.2 Granodiorite

Granodiorite is composed mainly of plagioclase, quartz, potassic feldspars, biotite and hornblende. In a thin-section zircon, apatite, titanite and opaques are the main accessory minerals. Plagioclase exhibits subhedral tabular crystals, ranging in composition

from oligoclase to andesine. Plagioclase crystals show albite-carlsbad and pericline twinning. Potassium feldspars are present as subhedral orthoclase crystals, showing simple twinning and corroded by quartz. Biotite forms subhedral to anhdral flakes of brownish color, strongly pleochroic from yellowish-brown to dark brown. Occasionally, they are altered to chlorite and iron oxides.

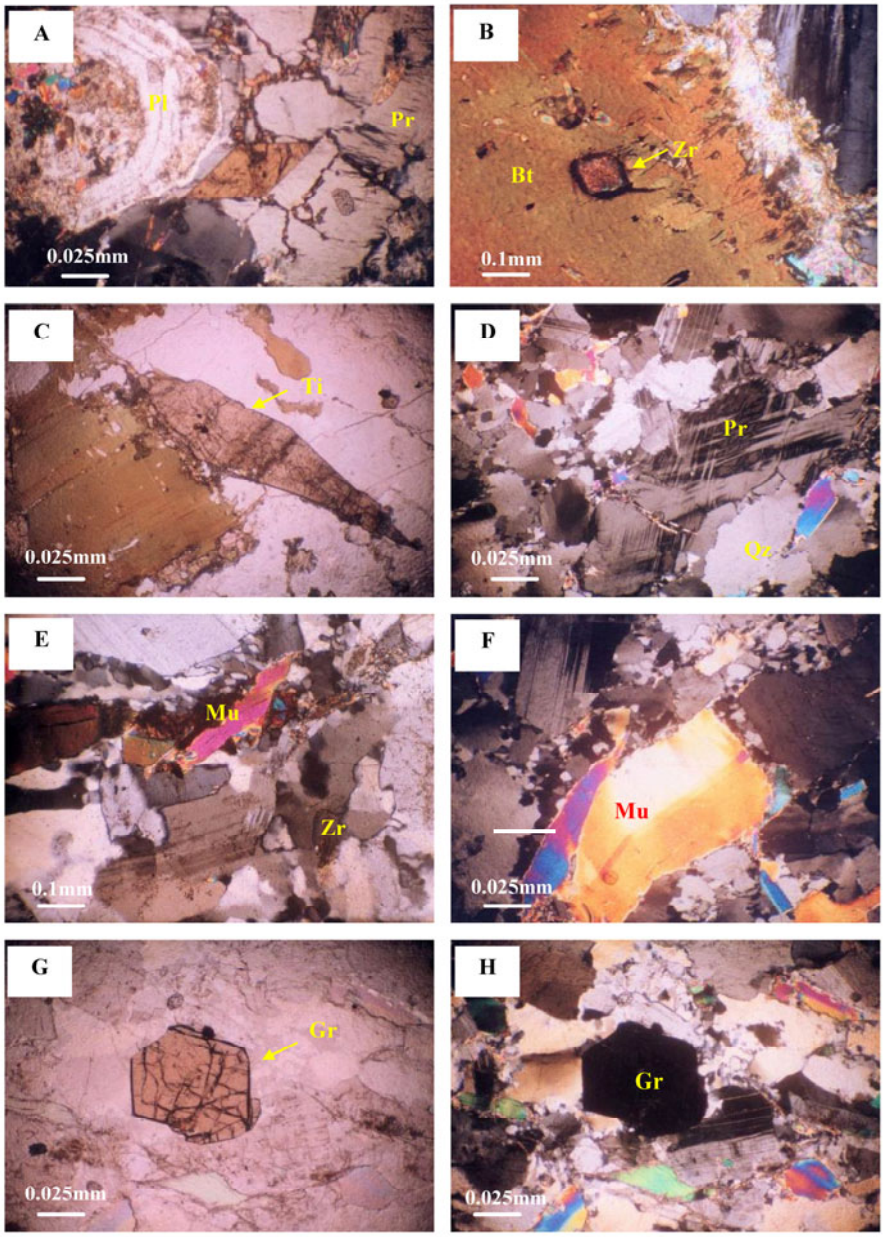

Fig. 2. A. Oscillatory zoning in plagioclase corroded by perthites and quartz in biotite granite (Crossed Nicols); B. metamict zircon within biotite crystal in biotite granite (Crossed Nicols); C. large titanite crystals associated with biotite flakies in biotite granite (Crossed Nicols); D. microcline crystals corroded by quartz and muscovite, garnet- muscovite granite (Crossed Nicols); E. zircon associated primary muscovite, garnet-muscovite granite (Crossed Nicols); F. primary muscovite invaded by secondary quartz, garnet-muscovite granite (Crossed Nicols); G. garnet crystal from garnet-muscovite granite (Polarized Light); H. the previous photo under Crossed Nicols. Pl. Plagioclase; Pr. perthite; Zr. zircon; Ti. titanite; Qz. quartz; Gr. garnet; Mu. muscovite; Bt. Biotite.

3.2 Biotite granites

Biotite granites generally form moderate to low relief, medium- to coarse-grained, pink to whitish-red in color and occur along the southern border of the map area as part of the Gabal Um Atali granite. The biotite granites carry several xenoliths of different shapes and sizes of the older granitoids. It is generally equigranular, sometimes porphyritic in texture and composed mainly of perthite, quartz, plagioclase and

biotite. Zircon, titanite, apatite and opaques are accessory minerals.

Alkali feldspar (mainly perthite) is the most dominant mineral that occurs as subhedral to anhedral prismatic crystals. It is represented by orthoclase perthite and microcline perthite. Quartz is less dominant than perthite and is found as subhedral to anhedral crystals. Plagioclase occurs as subheral to anhedral crystals and show clear lamellar and simple twinning (Fig. 2A).

Biotite occurs as flakes of brown-color, strongly pleochroic from yellowish-brown to dark-brown (Fig. 2A). Sometimes, they are altered to chlorite and iron oxides. Zircon is found as minute prismatic crystals occasionally enclosed in quartz, plagioclase and biotite (Fig. 2B). Titanite exhibits small anhedral to subhedral, highly cracked sphenoid crystals (Fig. 2C).

3.3 Muscovite granites

Muscovite granites form a small circular mass at the center of the mapped area. Generally, they are coarse-grained, high to moderate in relief and pink to reddish- white in color. They have intruded the diorite to granodiorite rocks and sent several apophasess into them. The rocks carry several xenoliths of various shapes and sizes of the older granitoids. They contain garnet as black inclusions. Alkali feldspars essentially consist of perthites, quartz, plagioclase, muscovite and rare biotite. Garnet, zircon, apatite, fluorite and opaques are accessories. Chlorite, sericite and kaolinite are secondary minerals. Alkali feldspars (mainly perthites) are represented by both microcline and orthoclase perthites. They are of a string, patchy and flame-like type (Fig. 2D). Microcline perthite is the most predominant mineral. Quartz occurs as subhedral to anhedral interstitial crystals between perthites and plagioclase. Plagioclase (albite to oligoclase) occurs as small euhedral crystals, commonly twinned and corroded by quartz and muscovite.

Muscovite occurs in the form of flakes. It corrodes plagioclase and perthite (Fig. 2E). It contains zircon, apatite and opaques as inclusions. Garnet occurs as subhedral to anhedral crystals. It is characterized by high relief, brownish tint, isotropism and contains inclusions of quartz and muscovite (Fig. 2E, F). Zircon occurs as euhedral to subhedral prismatic crystals, which is generally enclosed in quartz and muscovite (Fig. 2G, H). Apatite is rarely encountered and when present, it occurs as very thin colorless prismatic crystals of a very small size.

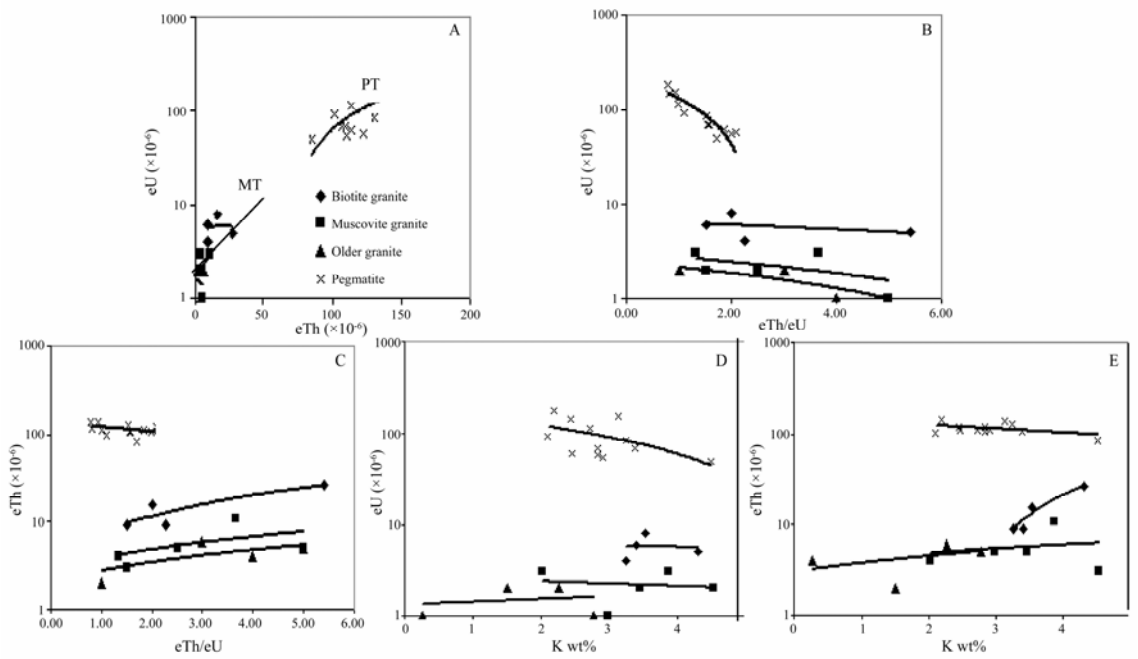

Fig. 3. Binary diagrams: A. eU vs. eTh; B. eU vs. eTh/eU; C. eTh vs. eTh/eU; D. eU vs. K wt%; E. eTh vs. K wt%. MT (magmatic trend) and PT (pegmatite trend) after Shaw (1968).

3.4. Pegmatites

Pegmatites are commonly encountered in the studied area. They are found as dykes and small bodies with dimensions ranging from 2 to 10 m in width and 10 to 500 m in length. (Fig. 1D). These rocks are very coarse-grained, mainly observed in the garnet muscovite granites near the contact with the older granitoids. They are composed mainly of megacrysts of potassic feldspar (70%), milky quartz (20%), and plagioclase (8%), together with small pockets of mica

(muscovite and biotite), as well as a reasonable amount of garnet. The accessory minerals are mainly zircon, fluorite, apatite, and xenotime. Field radiometric measurements indicated that the radioactivity of pegmatites is more than twice that of their enclosing country rocks.

4 Results and discussion

Uranium and thorium are generally enriched in the youngest, felsic and potassic members of igneous rocks (Rogers and Ragland, 1961). Most of the radioactive occurrences in the rocks are in muscovite granites and associated pegmatites. The radioelement measurements of the studied rock units are shown in Table 2.

Calibration of the instrument was carried out by using gamma emitting sources Co-57 (122.1 kV, set up in channel 122) and Cs-137 (661.6 kV, set up in channel 662) as follows:

(1) Calibration starts with the Cs-137 source (coarse adjustment) and then with Co-57 source (fine adjustment).

(2) The Cs-137 source is repeatedly used as minimum procedure.

(3) Since the electrical noise of the photomultiplier in the detector unit generates low amplitude pulses, the lower level discrimination of the instrument must be set up to the level of channel 40 in order to avoid such pulses as well as natural cosmic and X-rays from the registered signals.

The unknown samples were measured through the system and then related to the standards for U, Th, Ra, and K provided by the International Atomic Energy Agency (IAEA). The samples were measured two times 1000 second each, and then the average of the total counts was taken. These counts are input to a computer program (analysis) written using Pascal language (Matolin, 1990) which run under MS-Dos to calculate the concentrations of the radioelements (U, Th & Ra in $\times 10^{-6}$) and K (in %).

The U and Ra of the studied diorite to granodiorite rocks range from (1 to 2)$\times 10^{-6}$ and (1 to 3)$\times 10^{-6}$ with the average values of (1.5 and 2)$\times 10^{-6}$, respectively. The equivalent thorium ranges from (2 to 6)$\times 10^{-6}$ with an average of 4.3×10^{-6}. Potassium contents range from 0.3% to 2.8% with an average of 1.7%. The arithmatic means of U (1.5) and Th (4.3) in the older granitoids are lesser than those of the world averages (4.8×10^{-6} U and 17×10^{-6} Th) as is shown by Rogers and Adams (1969).

Table 1. Radionuclide contents in the studied granitoids and pegmatites of Wadi Khuda

Rock type	Sample No.	^{238}U ($\times 10^{-6}$)	^{232}Th ($\times 10^{-6}$)	^{226}Ra($\times 10^{-6}$)	^{40}K (wt%)	Th/U	U/K
Diorite to granodiorite	110	1	4	2	0.3	4	3.7
	251	2	2	3	1.5	1	1.3
	118	1	5	2	2.8	5	0.4
	115	2	6	1	2.3	3	0.9
	Average	1.5	4.3	2	1.7	3.3	1.6
Biotite granite	355	6	9	3	3.4	1.5	1.8
	340	8	16	4	3.5	2.0	2.3
	336	4	9	3	3.3	2.3	1.2
	342	5	27	8	4.3	5.4	1.2
	Average	5.8	15.2	4.5	3.6	2.8	1.6
Muscovite granite	351	2	3	2	4.5	1.5	0.4
	109	3	4	2	2.0	1.3	1.5
	353	2	5	1	3.5	2.5	0.6
	354	1	5	2	3	5.0	0.3
	143	3	11	2	3.9	3.7	0.8
	Average	2.2	5.6	1.8	3.4	2.8	0.7
Pegmatite	1P	69	107	53	3.4	1.6	20.4
	2P	70	110	68	2.8	1.6	24.7
	3P	115	114	79	2.7	1	42.3
	4P	147	120	109	2.5	0.8	59.8
	5P	94	102	63	2.1	1.1	44.8
	6P	182	144	133	2.2	0.8	82.7
	7P	86	131	71	3.3	1.5	26.5
	8P	155	142	123	3.1	0.9	49.4
	9P	56	111	44	2.9	2	19.2
	10P	59	123	46	2.8	2.1	20.9
	11P	62	114	47	2.5	1.8	25.1
	12P	50	85	32	4.5	1.7	11.1
	Average	95.3	116.9	72.3	2.9	1.4	35.6

Biotite granite contains U ranging from (4 to 8)$\times 10^{-6}$ with an average of 5.8×10^{-6}, while Th contents ranging from (9 to 27)$\times 10^{-6}$ with an average of 15.3×10^{-6}. The U contents in muscovite granites range from (1 to 3)$\times 10^{-6}$ with an average of 2.2×10^{-6} while Th contents range from (3 to 11)$\times 10^{-6}$ with an average of 5.6×10^{-6}. The arithmatic means of U and Th in the biotite granite are 5.8 and 15.2, respectively where garnet muscovite granite means are 2.2 and 5.6, respectively. The arithmatic mean of the biotite granites is similar to that of post-orogenic granites of

is similar to that of post-orogenic granites of Saudi Arabia (4.8×10^{-6} U and 14.2×10^{-6} Th) as determined by Stuckless et al., (1984) while the values of two mica granites are lesser than those of Stuckless et al. (1984). The relatively high values of U and Th in the studied younger granites are mainly related to the presence of radioactive accessory minerals (such as metamict zircon and apatite) observed in their thin sections and mineralogical studies as will be shown later. Equivalent uranium contents of anomalous pegmatite samples (U) vary between 50×10^{-6} and 182×10^{-6}, while their equivalent thorium (Th) varies from 85×10^{-6} to 144×10^{-6}. Generally, the average contents of U and Th are higher than those reported for silicic intrusive rocks (Adams et al., 1956) and more than those of uraniferous pegmatites given by Ford (1982) for the Wadi Misma pegmatite by El Aassy et al. (1998) and for the Gabal Um Dissi pegmatites by Ahmed and Abdel Warith (2003).

The U-Th diagram of the studied diorite to granodiorite rocks, biotite, muscovite granites (magmatic trend) and pegmatites (pegmatitic trend) show a positive correlation which indicates that the behavior of U and Th was controlled by post-magmatic processes (Fig. 3A) (Simpson et al., 1979). The variation of Th and U against Th/U ratio, respectively shows a negative correlation with U and an ill-defined relation with Th, which has confirmed the idea that U and Th enrichment in these anomalies was controlled by magmatic processes or deuteric ones (Fig. 3B, C) (Simpson et al., 1979). On the other hand, potassium shows an ill-defined relation with both U and Th, this is mainly due to the post-magmatic alteration processes causing alteration of feldspar into kaolinite as will be shown later (Fig. 3D, E). In pegmatites, the average Th/U (Table 1) is low (1.4) and the average U/K (35.6) is high, which suggests that uranium concentrating processes have not affected the pegmatites, therefore indicating a poor source-rock (Saunders, 1979; Stuckless et al., 1984).

Detailed mineralogical examinations of the studied pegmatites south of Wadi Khuda revealed the presence of secondary uranium minerals (kasolite and autunite), zircon, thorite, apatite, garnet and mica.

4.1 Secondary uranium minerals

The uranyl silicate minerals can be divided into several categories on the basis of their uranium and silicon ratios (Stohl and Smith, 1981). Three categories, with uranium to silicon ratios of 1:1, 1:3, and 2:1, are well defined and reported by Stohl (1974), and Stohl and Smith (1974). Kasolite is the member of the first group with uranium to silicon ratio 1:1. Kasolite is distinguished by its bright colors (canary lemon, yellow and brown of different intensities). These minerals are close in their physical properties and morphological features and characterized by their softness to crushing. However, kasolite grains compared to other uranium secondary minerals are relatively harder (Raslan, 2004). Kasolite is generally distinguished from the other uranium silicates by its crystal habit and luster. It is a hydrated silicate of lead and hexavalent uranium and is the only uranyl silicate with lead as major cation. These grains usually occur as massive granular form composed of druses of rod like crystals. They are characterized by their waxy or greasy luster (Fig. 4A). Pure crystals of kasolite were subjected to XRD analysis and the results are shown in Fig. 5A.

The SEM microphotographs and EDS analyses reflect the morphological features and chemical composition of these grains and show that it usually consists of clusters of rod -like crystals (Figs. 4B, C and 5B). EPMA analyses of the kasolite reflects the major elements in the mineral; UO_2 (49.24%), PbO (36.09%) and SiO_2 (10.23%) associated with quartz, minor amounts of LREE and Y were reported as minor elements in kasolite (Fig. 4D, Table 2). The composition of analyzed kasolite (Table 2) can be expressed in the following formula: $(Pb_{0.37}\sum REE_{0.01})_{\sum 0.38}O_3(U_{0.84})O_3\cdot 3(Si_{0.32})O_2\cdot 4H_2O$. The REEs occupy the Pb sites in the lattice.

Autunite crystals are generally characterized by their dull luster and present as soft aggregates of bright yellow colors (Fig. 4E). The SEM data (Fig. 5C) confirms the chemical composition of autunite. The major oxides in these crystals are UO_2 (65.57%), CaO (20.58%) and P_2O_5 (8.19%), together with minor amounts of FeO (1.76%), SiO_2 (2.54%), Na_2O (0.60%) and Al_2O_3 (0.76%).

4.2 Zircon-thorite association

Zircon occurs as euhedral prismatic grains characterized as being pale to deep brown in color and generally sub-translucent to opaque with dull luster. The most common habit is the bipyramidal form with various pyramidal faces. However, some zircon crystals are characterized by extremely short prisms, as being more or less equidimensional and exhibiting square cross section. The SEM data (Figs. 4F and 5D) reflect the chemical composition of zircon and its thorite inclusions. The SEM image and semiquantitative analysis shows that thorite consists essentially of ThO_2, SiO_2 and UO_2 together with minor amounts of Y, Ca, Mg, Fe, Zr, and Si. The EPMA analyses showed the thorite is composed mainly of ThO_2, SiO_2, and UO_2 (Table 2). Thorite was found as zonend crystals within zircon as indicated from Scanning Electron Microscope (SEM) analyses (Fig. 4G). The obtained EPMA for these inclusions reflects U-enrichment in

the cores of thorite grains than their rims (cryptic chemical zoning), where major elements in thorite core are ThO_2 (57.12%), SiO_2 (13.51%) and UO_2 (10.12%) but at the thorit rim are ThO_2 (58.54%), SiO_2 (13.79%) and UO_2 (7.92%), in addition to LREE and Y (Fig. 5E and Table 2). The average composition of the analyzed thorite (Table 2) can be expressed in the following formula: $(Th_{1.05}Y_{0.195}\sum REE_{0.19}U_{0.15}Al_{0.029}Pb_{0.005})_{\sum 1.62}(Si_{0.42}P_{0.02})O_4$. Uranium, rare earths, Y, Pb and Al substitute Th site in the crystal lattice. PO_4 is known to substitute for SiO_4.

Table 2. Microprobe analyses of kasolite and thorite in the granitic pegmatites of the Khuda area

SiO_2	10.23	13.51	13.79
Na_2O	0.07	0.03	n.d
Al_2O_3	n.d	1.52	1.26
HfO_2	0.26	0.09	0.06
P_2O_5	0.07	0.73	0.82
CaO	n.d	0.52	0.48
FeO	0.013	0.07	0.04
Y_2O_3	0.020	6.26	7.08
Ce_2O_3	0.16	n.d	0.28
Sm_2O_3	n.d	0.34	n.d
Pr_2O_3	n.d	n.d	0.07
Eu_2O_3	n.d	0.27	0.08
Gd_2O_3	0.14	0.03	n.d
Er_2O_3	n.d	1.69	1.65
Dy_2O_3	n.d	1.35	1.41
Yb_2O_3	n.d	3.10	2.90
Nb_2O_5	0.05	n.d	n.d
UO_2	49.24	10.12	7.92
ThO_2	n.d	57.12	58.54
PbO	36.09	0.53	0.55
F	n.d	4.56	5.20
Total	96.34	101.84	102.13
Si	0.32	0.42	0.42
Na	0.002	0.001	0.00
Al	0.00	0.032	0.026
Hf	0.003	0.001	0.001
P	0.002	0.018	0.021
Ca	0.00	0.015	0.013
Fe	0.00	0.002	0.001
Y	0.001	0.183	0.207
Ce	0.005	0.00	0.008
Sm	0.00	0.01	0.00
Pr	0.00	0.00	0.003
Eu	0.00	0.008	0.002
Gd	0.004	0.001	0.00
Er	0.00	0.05	0.05
Dy	0.00	0.04	0.04
Yb	0.00	0.09	0.08
Nb	0.002	0.00	0.00
U	0.84	0.17	0.135
Th	0.00	1.042	1.068
Pb	0.37	0.005	0.006

n.d. Not detected.

The studied thorite is sporadic in U distribution, suggesting non-uniform redistributions of UO_2 within thorite during post magmatic processes. Several authors reported the presence of thorite inclusions in rare metal mineralization and accessory heavy minerals separated from some Egyptian pegmatites (Raslan et al., 2010; Ali et al., 2005; Abdel Warith et al., 2007).

4.3 Biotite

Dark biotite flakes are the most dominant mineral in the heavy fractions separated from the studied pegmatites. They occur as flexible plates of dark brown color, partially chloritized and usually stained with iron oxides (Fig. 4H).

4.4 Apatite

Under binocular microscope, apatite grains are mainly massive with well rounded to subrounded shapes. The color of apatite grains generally varies from pale yellow to dark brown. The EDS analysis (Fig. 5F) reflects the chemical composition of apatite associated with a minor amount of uranium and manganese. Uranium usually substitutes for Ca in fluor-apatite. The intensity of the color in fluor-apatite increases with increasing Mn content (Deer et al., 1992).

4.5 Garnet

Garnet occurs as reddish-brown transparent to translucent massive grains of granular form, possessing vitreous luster and being usually hard. Semiquantitative analyses of some grains (Fig. 5G) reflect the chemical composition of garnet.

5 Conclusions

Most of the radioactive occurrences in the basement rocks of Egypt are present in the granites and associated pegmatites. Radioactive pegmatites have been recorded in many localities in the Eastern Desert of Egypt (Sayyah et al., 1993; Ibrahim et al., 1997; Ali, 2001; Ibrahim et al., 2001; Ali et al., 2005; Abdel Warith et al., 2007; Raslan et al., 2010). Also, several studies worldwide have revealed the presence of granite-pegmatite-hosted rare-metal mineralizations (Matsubara et al., 1995; Hanson et al., 1998; Erict, 2005; William et al., 2006; Pal et al., 2007). Although pegmatites have been considered as favorable environments of uranium and thorium accumulation (Page, 1950), they are generally considered as poor mining targets (Gaberlman, 1977).

The granitic rocks of the Wadi Khuda area have been subdivided according to their field relations, petrography and their radioactive characteristics into two magmatic groups: Group I (diorite and granodiorite)

and Group II (biotite granite and garnet-muscovite granites) in addition to post granite dykes and veins.

The distribution of both U and Th in the studied pegmatites and their host granites is generally controlled by the distribution of their mineral bearers. Radioelement contents of the younger granites are low but those of pegmatites are high, this is attributed to the presence of radioactive minerals. The average eTh/eU ratio is lower in the pegmatites (<2) than in the older and younger granites (>2), indicating addition of U and manifesting remobilization and redistribution during diagenetic processes.

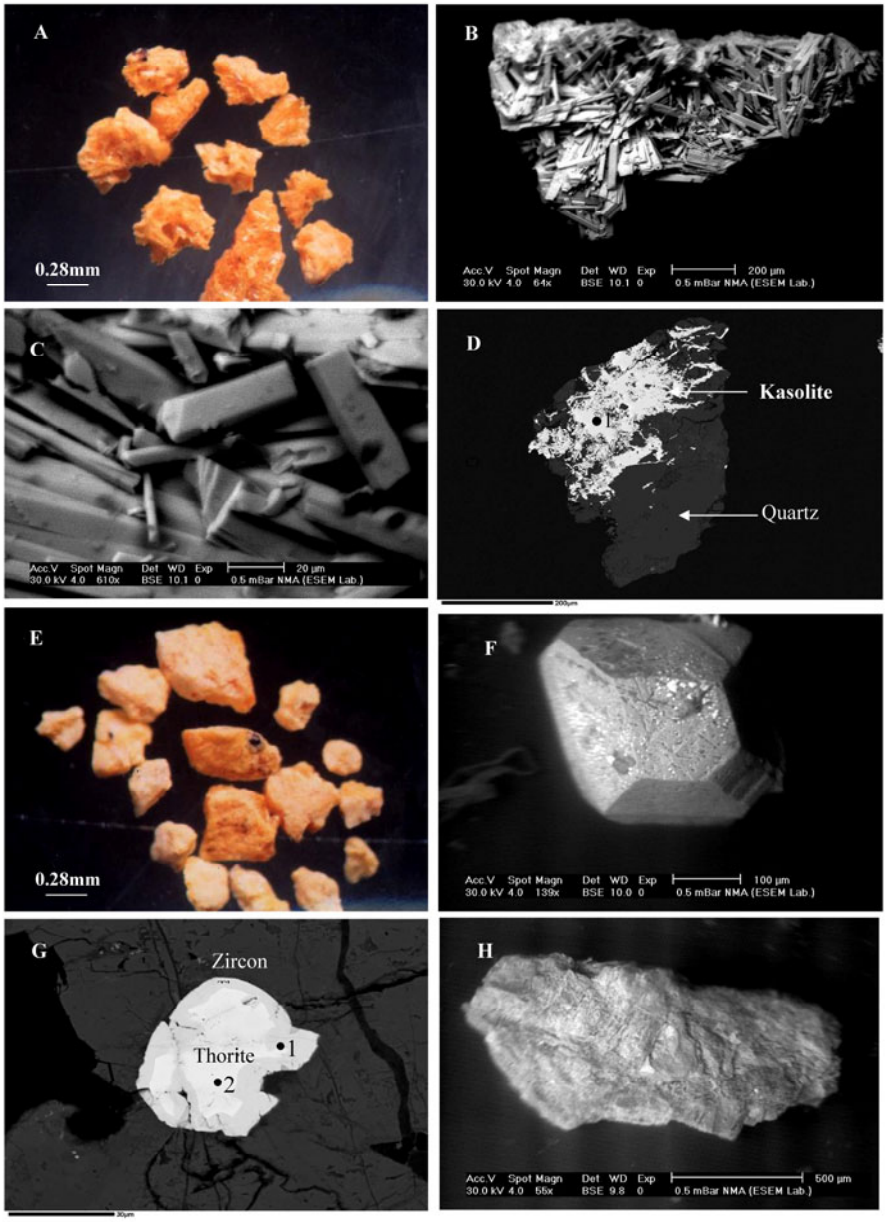

Fig. 4. A. Kasolite crystals of rod-like aggregates (binocular microscope); B and C. SEM-BSE images illustrating the micromorphological features of kasolite; D. SEM-BSE image of kasolite associated with quartz; E. massive yellow grains of autunite (binocular microscope); F & G. SEM-BSE images for zircon containing thorite inclusions, and zoned thorite within zircon (analyses 1 and 2); and H- BSE image for biotite.

The average contents of eU and eTh increase gradually from the older granitoids (1.5×10^{-10} eU and 4.25×10^{-10} eTh) to biotite granite (5.75×10^{-10} eU & 15.25×10^{-10} eTh) against lesser contents in garnet muscovite granite (2.2×10^{-10} eU and 5.6×10^{-10} eTh). The average contents of eU and eTh of anomalous pegmatites are 90.3×10^{-10} and 116.9×10^{-10}, respectively, indicating their uraniferous nature. Although the studied pegmatites are anomalous in terms of uranium concentrations, the potential for finding ore deposits are low. This is due to their low eTh/eU ratio (average 1.4) and high eU/K (average 32.86). Post-magmatic redistribution of U (mobilization) as indicated from eU and eTh with eTh/eU ratio cross

plot, desequilirium state between eU and Ra (eU/Ra>1), low eTh/eU ratio, high eU/K ratio and zircon-thorite intergrowths could be considered as the criteria for uranium prospecting in other areas because mobilized uranium may be concentrated into deposits within or near the source rock (Osmond et al., 1999; Dawood et al., 2004).

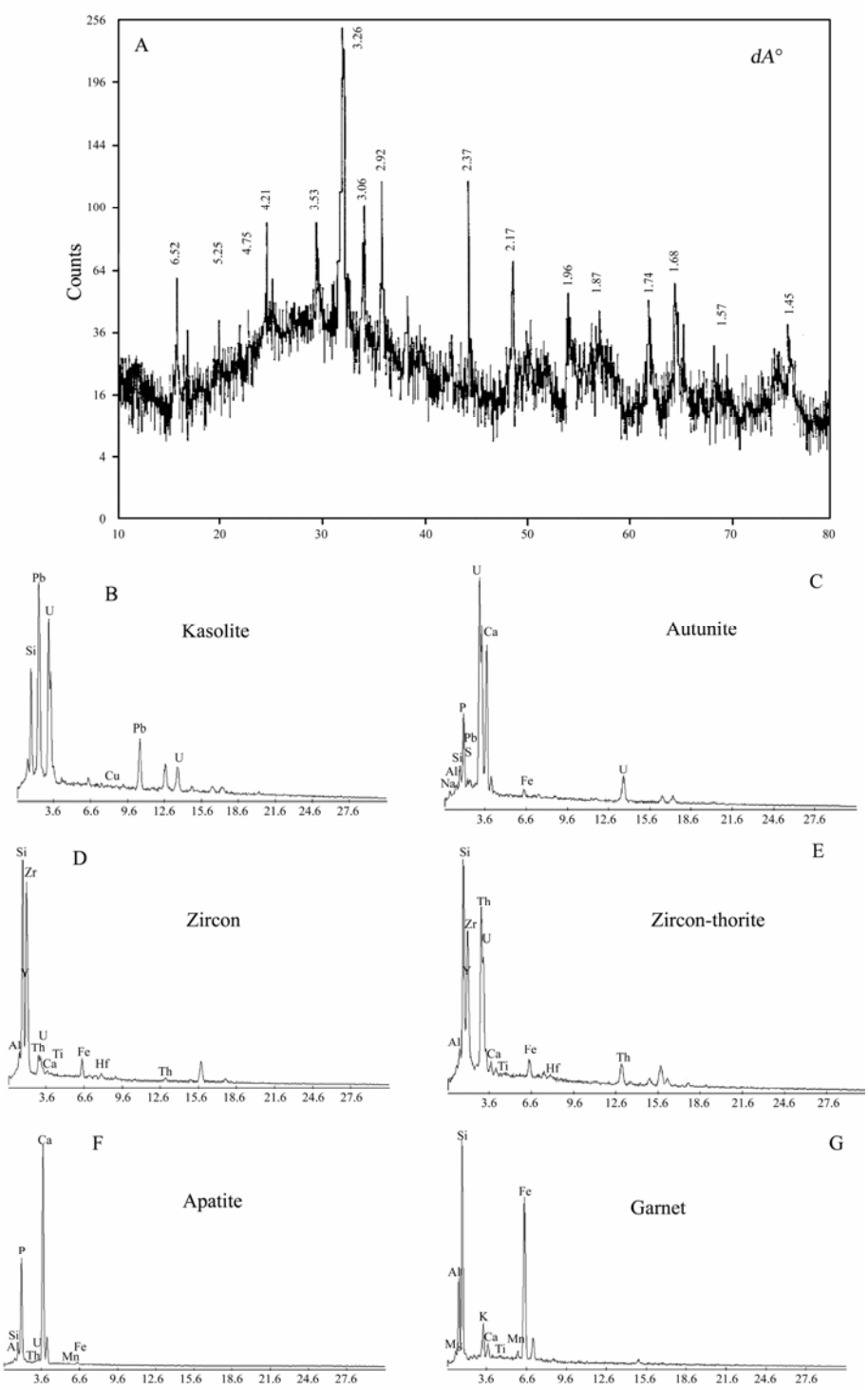

Fig. 5. A. XRD pattern of kasolite; B, C, D, E, F and G. EDS spectra of kasolite, autunite, zircon and its thorite inclusions, apatite and garnet, respectively.

Electron microprobe analyses of kasolite suggest the following formula: $(Pb_{0.37}\sum REE_{0.01})_{\sum 0.38}O_3(U_{0.84})O_3{\cdot}3(Si_{0.32})O_2{\cdot}4H_2O$. The average composition of the analyzed thorite can be expressed as the following formula: $(Th_{1.05}Y_{0.195}\sum REE_{0.19}U_{0.15}Al_{0.029}Pb_{0.005})_{\sum 1.62}(Si_{0.42}P_{0.02})O_4$. EMPA analyses show distinct cryptic chemical zoning within thorite where UO_2 decreases from core to rim. This feature in thorite is sporadic,

suggesting non-uniform redistributions of UO_2 within thorite during magmatic processes.

Magmatic mineralization is evidenced by the presence of thorite and normal zircon, whereas hydrothermal mineralization is indicated by the formation of secondary minerals such as kasolite, autunite and zircon-thorite intergrowth. Radiometric and mineralogical studies indicated that radioactive mineralization is not only magmatic, but also post-magmatic, in addition to the effects of weathering and meteoric water.

Acknowledgements Microprobe analyses were carried out at the University of New Brunswick (UNB), Canada. The authors sincerely thank Dr. Douglas Hall and Prof. Dr. David Lenz for their interest and providing EMPA analyses.

References

Abdalla H.M. and El Afandy A.H. (2003) Contrasting mineralogical and geochemical characteristics of two A-type pegmatite fields, Eastern Desert, Egypt [J]. *Egyptian Mineralogists*. **20**, 287–328.

Abdel Karim A.M. and E. Arva Sos. (2000) Geochemical characteristics and K-Ar ages of some granitoid from South Eastern Desert, Egypt [J]. *Egyptian Journal of Geology*. **44/1**, 305–318.

Abdel Khalek M.L., Takla M.A., Sehim A.A., Abdel wahed M., Hamimi Z., and Sakran Sh.M. (1999) Tectonic evolution of the Shield rocks, East Wadi Beitan area, South Eastern Desert, Egypt [J]. *Egyptian Journal of Geology*. **43/1**, 1–25.

Abdel Warith A., Raslan M.F., and Ali M.A. (2007) *Mineralogy and Radioactivity of Pegmatite Bodies from the Granitic Pluton of Gabal Um Tager El-Tahtani Area, Central Eastern Desert, Egypt* [C]. The 10th International Mining, Petroleum, and Metallurgical Engineering Conference, Mining, Code No. M3, Faculty of Engineering-Assuit University.

Adams J.A.S., Osmond J.K., and Rogers J.J.W. (1956) "The geochemistry of thorium and uranium". In *Physics and Chemistry of the Earth* [M]. **2**, 298–348.

Ahmed F.Y. and Abdel Warith A. (2003) *Radioactive Studies of Gabal Um Dissi Younger Granites and the Associated Pegmatites, North Eastern Desert, Egypt, Al Azhar Bulletien of Science* [C]. pp.25–27, 31–43. Proc. of 5th Int. Sci. Conf.

Ali M.A. (2001) *Geology, Petrology and Radioactivity of Gabal El-Sibai Area, Central Eastern Desert, Egypt* [D]. pp.300. Ph.D Thesis, Cairo University.

Ali M.A., Raslan M.F., and El-Feky M.G. (2005) *Radioactivity and Mineralogy of Some Pegmatite Bodies from Gabal Al-Farayid Granites, South Eastern Desert, Egypt* [C]. The 9th International Mining, Petroleum, and Metallurgical Engineering Conference February 21–24, 2005, Faculty of Engineering-Cairo University.

Cerny P. (1990) Distribution, affiliation and derivation of rare-element granite pegmatites in Canadian Shield [J]. *Geologische Rundschau*. **79**, 183–226.

Dawood Y.H., Abd El-Naby H.H., and Sharafeldin A.A. (2004) Infuence of the alteration processes on the origin of uranium and europium anomalies in trachyte, central Eastern Desert, Egypt [J]. *J. Geochem. Explor*. **88**, 15–27.

Deer W.A., Howie R.A., and Zussman J. (1992) *Rock Forming Minerals, Vol. 5. Non Silicates* [M]. John Wiley and Sons, New York.

Dixon T.H. (1981) Age and chemical characteristics of some Pre-Pan-African rocks in the Egyptian shield [J]. *Precambrian Res*. **14**, 119–133.

El Aassy I.E., Shazly A.G., Hussein H.A., Heikel M.T.S., and El Galy M.M. (1998) P*egmatites of Nuweiba-Dahab Area, West Gulf of Aqaba, Sinai, Egypt: Field Aspects, Mineralogy, Geochemistry and Radioactivity* [C]. pp.139–151. 3rd Conf. of Geoch. Alex. Univ. V.I., Geoch. of igneous rocks and Geochemical exploration, Alex.

El-Manharawy M.S. (1977) *Geochronological Investigation of Some Basement Rocks in Central Eastern Desert, Egypt Between Lat. 25° and 26°N* [D]. pp.216. Unpub. Ph. D. Thesis, Cairo University, Egypt.

El-Ramly M.F. and Akaad M.K. (1960) The basement complex in the Central Eastern Desert of Egypt between lat. 24°30′ and 25°40′ N [J]. *Geological. Survey, Egypt*. (8), 35.

Ford K.L. (1982) Uraniferous pegmatites of the Sharbot Lake area, Ontario. In *Uranium in Granites* (ed. Maurice Y.T.) [M]. pp.81–23, 125–138. Geol. Surv. of Canada.

Erict T.S. (2005) Identification and alteration trends of granitic-pegmatite-hosted (Y, REE, U, Th)-(Nb, Ta, Ti) oxide minerals: A statistical approach [J]. *Canadian Mineralogist*. **43**, 1291–1303.

Gaberlman J.W. (1977) Migration of uranium and thorium exploration significance [J]. *American Association for Petroleum Geologists Bulletin, Studies in Geology*. APPG, USA. (3), 168.

Hanson S.L., Simons W.B., and Falster (1998) A.U., Nb-Ta-Ti oxides in granitic pegmatites from the Topsham pegmatite district, South Maine [J]. *The Canadian Mineralogist*. **36**, 601–608.

Hassan M.A. and Hashad A.H. (1990) Precambrian of Egypt. The anorogenic alkalic rocks, South Eastern Desert, Egypt [J]. *Annal Geological Survery 9, Egypt*. 81–101.

Hume W.F. (1935) *Geology of Egypt. Vol. II, Part II. The Later Plutonic and Intrusive Rocks. Geological Survery Egypt* [M]. pp.301–688. Government Press, Cairo.

Hussein A.A., Ali M.M., and El-Ramly M.F. (1982) A proposed new classification of the granites of Egypt [J]. *Journal of Volcanic and Geothermal Research*. **14**, 187–198.

Ibrahim M.E., Shalaby M.H., and Ammar S.E. (1997) Preliminary studies on some uranium and thorium bearing pegmatites at G. Abu Dob, Central Eastern Desert, Egypt [J]. *Proc. Egypt. Acad. Sci*. **47**, 173–188.

Ibrahim M.E., Saleh G.M., and Abd El-Naby H.H. (2001) Uranium mineralization in the two mica granite of Gabal Ribdab, South Eastern Desert, Egypt [J]. *Appl. Radiat. Isot*. **55/6**, 123–134.

Matolin M.M. (1991) "*Construction and Use of Spectrometric Calibration Pads", Laboratory of Gamma-ray spectrometry, N.M.A., Egypt* [R]. A report to the Government of the Arab Republic of Egypt. Project Egy., 4, 030-03, IAEA.

Matsubara S., Kato A., and Matsuyama F. (1995) Nb-Ta minerals in a lithium pegmatite from Myokenzan, Ibaraki Prefecture, Japan [J]. *Mineralogical Journal*. **17**, 338–345.

Moussa E.M.M., Stern R.J., Manton W.I., and Ali K.A. (2008) Shrimp zircon dating and Sm/Nd isotopic investigations of Neoproterozoic granitoids, Eastern Desert, Egypt [J]. *Precamb. Res*. **160**, 341–356.

Osmond J.K., Dabous A.A., and Dawood Y.H. (1999) U series age and origin of two secondary uranium deposits, central Eastern Desert, Egypt [J]. *Economic Geology*. **94**, 273–280.

Page L.R. (1950) Uranium in pegmatites [J]. *Econ. Geol*. **45**, 12–34.

Pal D.C., Mishra B., and Bernhardt H.J. (2007) Mineralogy and geochemistry of pegmatite-hosted Sn-, Ta- Nb-, and Zr- Hf-bearing minerals from the southeastern part of the Bastar-Malkangiri pegmatite belt, Central India [J]. *Ore Geology Reviews*. **30**, 30–55.

Raslan M.F. (2004) Physical properties of kasolite from Gabal Gattar uranium prospect, North Eastern Desert, Egypt [J]. *Jour. Egyp. Mineralogist* (in press).

Raslan M.F., El Shall H.E., Omar S.A., and Daher A.M. (2010) Mineralogy of polymetallic mineralized pegmatite of Ras Baroud Granite, Central Eastern Desert, Egypt [J]. J*ournal of Mineralogical and Petrological Sciences*. **105** (3), 123-134.

Rogers J.J.W. and Adams J.A.S. (1969) Uranium and thorium. In *Handbook of Geochemistry* (ed. Wedepohl K.H.) [M]. VII-3, 92-B-1 to 92-0-8 and 90-B-1 to 90-0-5, Springer Verlag, Berlin.

Rogers J.J.W. and Ragland P.C. (1961) Variation of thorium and uranium in selected granitic rocks [J]. *Geochim. et Cosmochim. Acta*. **25**, 99–109.

Saunders D.F. (1979) Characterization of uraniferous geochemical provinces by aerial gamma-ray spectrometry [J]. *Min. Eng*. **31**. 1715–1722.

Sayyah T.A., Assaf H.S.A., bdel Kader Z.M., Mahdy M.A., and Omar S.A. (1993) New Nb-Ta occurrence in Gebel Ras baroud, Central Eastern Desert [J]. *Egyptian Mineralogist*. **5**, 41–55.

Shaw D.M. (1968) A review of K-Rb fractionation trends by covariance analyses [J]. *Geochim. et Cosmochim. Acta*. **32**, 573–600.

Shurmann H.M.E. (1966) *The Precambrian Along the Gulf of Suez and the Northern Part of the Red Sea* [M]. E.J. Brill, Leiden, Netherlands.

Simpson P.R., Brown G.C., Plant J., and Ostle D. (1979) Uranium mineralization and granite magmatism in the British Isles [J]. *Phil. Trans. R. Soc. London*. **A.291**, 385–412.

Stohl F.V. (1974) *The Crystal Chemistry of the Uranyl Silicate Minerals* [D]. Ph.D. Thesis, The Pennsylvania State University, University Park.

Stohl F.V. and Smith D.K. (1974) T*he Crystal Chemistry of the Uranyl Silicate Minerals* [C]. (abstr.) American Crystallographic Association Meeting, Program and Abstracts Ser. 2, **2**, 271.

Stohl F.V. and Smith (1981) *The Crystal Chemistry of the Uranyl Silicate Minerals* [M]. Department of Geosciences, the Pennsylvania State University, University Park. Pennsylvania.

Stuckless J.S., Nkomo I.T., Wenmer D.B., and Van Trump G. (1984) Geochemistry and uranium favourability of the postorogenic granites of the north-eastern Arabian Shield, Kingdom of Saudi Arabia [J]. *Bull Fac. Earth Sci.* King Abdel Aziz Univ. **6**, 195–209.

William S.B., Hanson S.L., and Falster A.U. (2006) Samarskite-Yb: A new species of the samarskite group from the Little Patsy pegmatites, Jefferson County, Colorado [J]. *Canadian Mineralogist*. **44**, 1119–1125.